Int J Adv Manuf Technol (2014) 71:1929–1938
DOI 10.1007/s00170-014-5625-x

ORIGINAL ARTICLE

# Wear of diamond grinding wheel in ultrasonic vibration-assisted grinding of silicon carbide

**Kai Ding · Yucan Fu · Honghua Su · Xiaobei Gong · Keqin Wu**

Received: 24 July 2013 / Accepted: 13 January 2014 / Published online: 28 January 2014


**Abstract** It is recognized that grinding efficiency and ground surface quality are determined by grinding wheel performance. Additionally, the investigation on wear behavior is essential for evaluating the grinding wheel performance. There is a lack of research on the tool wear behavior during ultrasonic vibration-assisted grinding (UAG), whose grain motion trajectory differs from that in conventional grinding (CG). In the present work, CG and UAG tests of silicon carbide (SiC) were conducted in order to investigate the effects of ultrasonic vibration on the tool wear through tracking observation of grains. Meanwhile, the grinding forces and ground surface roughness correlated to the tool wear stages were studied. The results demonstrated that the main wear types during UAG were micro-fracture and macro-fracture which caused the wheel sharpening, while during CG, the main wear type was attritious wear that made the wheel blunt. As a result, UAG obtained lower and more stable grinding forces while slightly rougher ground surface in comparison with CG.

**Keywords** Silicon carbide · Ultrasonic vibration-assisted grinding · Tool wear · Grinding force · Surface roughness

## 1 Introduction

Silicon carbide (SiC) is one of the most ideal materials for space reflection mirrors due to its high specific stiffness, low thermal deformation coefficient, and low density [1–3]. Generally, optical components are lapped and polished to meet quality requirements. However, this complicated process leads to high cost and low efficiency [4–6]. Although grinding process with a diamond grinding wheel is applied to improve the machining efficiency, some problems are still present. For example, the rapid blunting and wear of diamond abrasives on the wheel surface will cause frequent dressing [7]. Additionally, for super-abrasive wheels, truing and dressing always generate pollution of the working environment and cause high wear of truing/dressing tools and mechanical damage of the abrasive grains [8]. Thus, it is urgent to develop a kind of effective machining technology for SiC.

Ultrasonic vibration-assisted grinding (UAG) is a kind of hybrid process that combines diamond grinding and ultrasonic machining [9, 10]. It has been applied to develop effective and high-quality grinding technology for hard-to-machine materials in different modes, especially for hard and brittle materials as described in the literature [11–14]. According to the vibration mode, UAG includes one-dimensional UAG and two-dimensional UAG [7, 13]. During one-dimensional UAG, the machining performance is determined by whether the vibration direction is parallel or vertical to the ground surface. Liang et al. [15] revealed that UAG can reduce the grinding forces slightly and improve the surface roughness compared with conventional grinding (CG) when the vibration direction was parallel to the ground surface. Uhlmann [16] conducted UAG and CG tests of advanced ceramics, and during UAG, the vibration direction was vertical to the ground surface. The results suggested that UAG can reduce the grinding forces apparently without causing remarkable subsurface damage while obtaining a slight increasing ground surface roughness in comparison with CG.

Yan et al. [17] conducted a two-dimensional UAG in which the workpiece vibrates simultaneously in two directions (i.e., vertical and parallel to the ground surface). The results suggested that it can achieve better surface quality and may improve the material removal rate in comparison with CG. Liang et al. [15] also reported that the grinding forces are

K. Ding · Y. Fu (✉) · H. Su · X. Gong · K. Wu
College of Mechanical and Electrical Engineering, Nanjing University of Aeronautics and Astronautics, Nanjing 210016, China
e-mail: yucanfu@nuaa.edu.cn

decreased by 30 % during two-dimensional UAG compared with CG. In summary, UAG including the vibration vertical to the ground surface can reduce the grinding forces significantly, i.e., it has great potential to realize effective machining of SiC.

It is generally recognized that grinding forces and machining quality are determined by tool performance. Therefore, it is very important to study the wear behavior of the grinding wheel to control the machining quality and efficiency. Malkin [18] concluded that there were three main wear types of the grinding wheel during CG, i.e., attritious wear, grain fracture, and bonding fracture. While during UAG, different kinematic characteristics will cause different types of wear behavior in comparison with CG. Zeng et al. [19] conducted rotary ultrasonic machining (RUM) tests on SiC and studied the tool wear types. Their results demonstrated that the tool wear process on the end face contained two stages: the first was attritious wear, and the second was bonding fracture; thus, the grinding forces increased firstly and then decreased. But, different views also exist in other literature. Mult et al. [20] studied the differences between UAG and CG through grinding tests of ceramics and indicated that the portion of grain splintering increased while the portion of grain flattening decreased during UAG than during CG. As a result, the grinding forces were reduced at the same material removal rates, while the ground surface deteriorated simultaneously. In summary, the results are not uniform in different literature for their lack of the detailed study on the grain wear process and final wear types. Furthermore, no interpretation on the grain wear is stated in essence.

To achieve consensus of the tool wear behavior during the one-dimensional UAG (the vibration is vertical to the ground surface), grain tracking observation is adopted to reflect the whole wear process of the tool in this study. In particular, the UAG and CG experiments of SiC are conducted with metal-bonded diamond wheels. During the experiments, grain tracking observation by optical microscopy is carried out several times after a certain volume material removal. The tool wear behavior during UAG and its effects on the grinding forces, ground surfaces roughness, and topographies is studied based on these results and on the kinematics analysis of the grains.

## 2 Kinematic analysis of the ultrasonic vibration-assisted grinding process

The UAG process is illustrated in Fig. 1. The diamond wheel rotates with a certain speed at the same time vibrates along the axial in a high frequency. Additionally, it keeps moving along the workpiece surface simultaneously to fulfill grinding. During UAG, the motion trajectory of a single diamond grain can be described by Eq. 1:

$$\begin{cases} X = R\cos(\omega t) + v_w t \\ Y = R\sin(\omega t) \\ Z = A\sin(2\pi f t) \end{cases} \quad (1)$$

where $R$ is the grinding wheel radius, $A$ is the amplitude of vibration, $\omega$ is the angular velocity, $v_w$ is the feed rate, $f$ is the vibration frequency, and $t$ is the time.

According to Eq. 1, the motion trajectory of a single grain during UAG is a 3D sine curve as drawn in Fig. 2 by MATLAB. Meanwhile, the motion trajectory of a single grain during CG is also shown in this figure for comparison. Define $\lambda$ as the wavelength of the 3D sinusoidal curve, and it can be described by Eq. 2:

$$\lambda = (v_s + v_w)/f \quad (2)$$

where $v_s$ is the grinding speed. According to the experiment conditions in this study, $\lambda$ is about 0.3 mm.

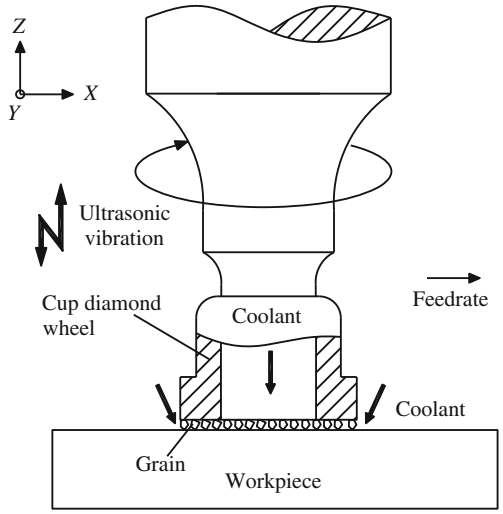


**Fig. 1** Illustration of UAG

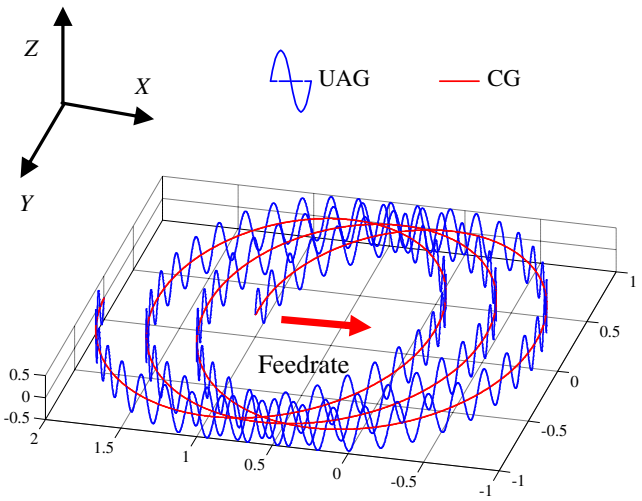


**Fig. 2** Grain motion characteristics of UAG and CG

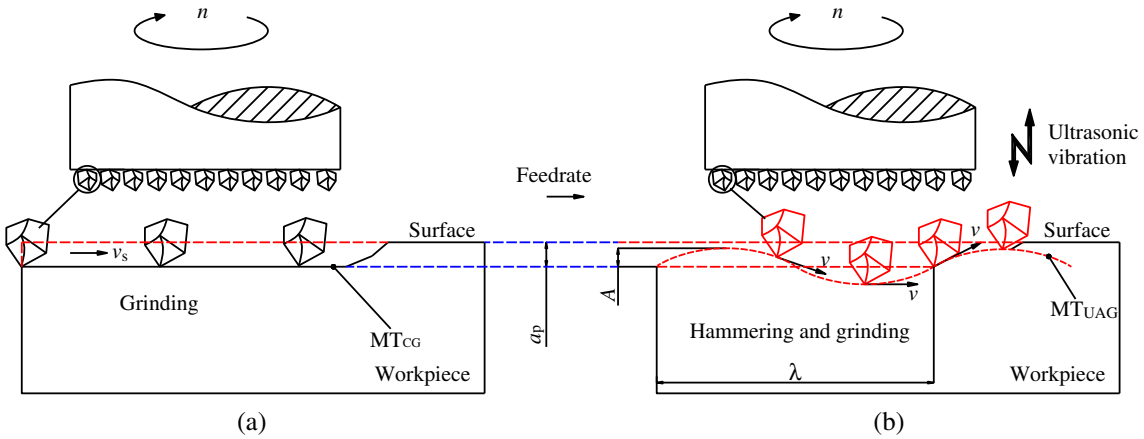


**Fig. 3** Ground surface generation process in **a** CG and **b** UAG

Under the same nominal grinding depth $a_p$, the CG motion trajectory ($MT_{CG}$) and UAG motion trajectory ($MT_{UAG}$) generated on the ground surface are shown in Fig. 3. During CG, the grinding depth is stable, while during UAG, the actual grinding depth is determined by the amplitude $A$ and nominal grinding depth $a_p$ collectively. As can be seen in Fig. 3b (because $\lambda$ is very small, a waveform is considered as a 2D sine curve to simplify the analysis in this figure), as long as the grinding depth $a_p$ is smaller than the amplitude $A$, a complete contact disruption between the grain and ground surface occurs in every motion cycle. Otherwise, no complete contact disruption would occur, but actual grinding depth will change all the time, which is also different from CG. In any case, hammering and grinding are generated simultaneously during UAG due to change of the actual grinding depth.

## 3 Experimental setup and procedures

The UAG and CG tests were carried out in a DMG Ultrasonic 20 Linear high-speed machining center. Figure 4 illustrates the experimental setup. A grinding wheel is fixed on the ultrasonic tool holder, which contains a secondary coil, a piezoelectric ceramic transducer, and an amplitude transformer. During UAG, an ultrasonic generator converts industrial electric signal into high-frequency (about 20–30.4 kHz) electric signal and then the high-frequency signal is transferred to the primary coil located at the end of the spindle and the secondary coil which is connected with the piezoelectric ceramic transducer. The piezoelectric ceramic transducer converts the electric energy into a mechanical energy, which is then amplified and transferred to the end face of the tool by the amplitude transformer horn. Along with rotation and feed motion of the grinding wheel, UAG can be executed. Shut down of the ultrasonic vibration system through a program is done when CG is conducted.

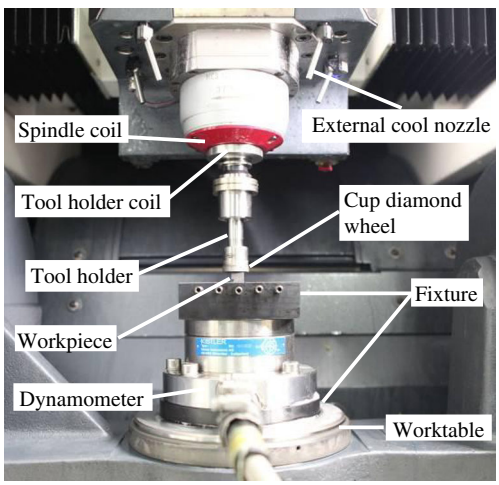


**Fig. 4** The experimental setup

The workpiece material was non-pressurized sintering SiC. The workpiece was bonded to the fixture by paraffin. The dimension of the workpiece was 30 mm×10 mm×10 mm. Two sintered cup diamond wheels (Schott, Germany) were used in the experiments, one was for UAG and the other was for CG. The outer diameters of the wheels were Ø24 mm, and the wall thicknesses were 2 mm. The grain size was 91 μm in average. Infeed grinding was adopted both in UAG and CG. The two wheels were sharpened by an abrasive stone before

**Table 1** Experimental conditions

| Condition | Feature |
|---|---|
| Vibration conditions | Frequency $f$ = 21.5 kHz, amplitude $A$ = 4 μm |
| Coolant | Castrol 9954, emulsion 5 %, pressure: external cooling 4 bar, inner cooling 10 bar |
| Sharpening conditions | Sharpening tool: abrasive stone (SiC), feed speed $v_w$ = 300 mm/min, grinding speed $v_s$ = 6.3 m/s, depth of cut $a_p$ = 0.5 mm, total depth of cut $a_{pT}$ = 9 mm |
| Grinding conditions | Feed speed $v_w$ = 200 mm/min, grinding depth $a_p$ = 20 μm, grinding speed $v_s$ = 6.3 m/s, grinding width $a_e$ = 10 mm |

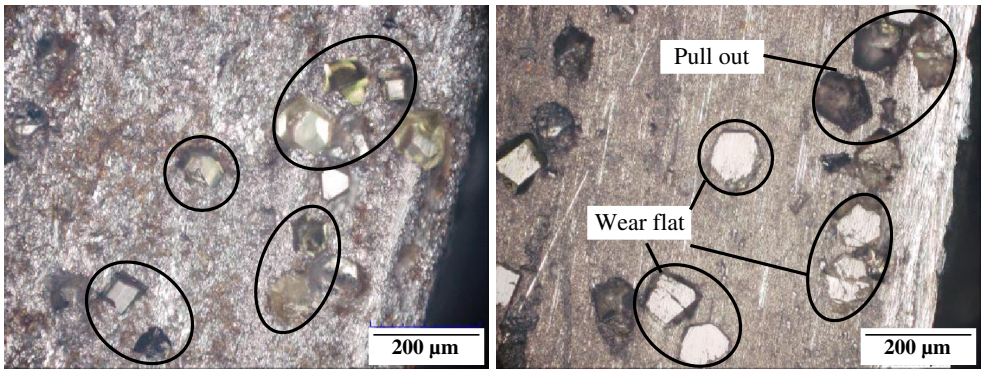


(a) Initial topography (b) Topography after 60 passes

**Fig. 5** Topography of the tool surface for CG (×350). **a** Initial topography, **b** topography after 60 passes

the experiments and then typical grains which possessed integrated shapes and certain protrusion were selected to be signed as the tracking targets through an optical microscopy. These grains were observed when a certain volume material was removed, and other parameters such as grinding forces and ground surface roughness were measured simultaneously. The sharpening conditions and grinding conditions are summarized in Table 1.

The vibration frequency and amplitude of the tool end face were measured by a Polytec single-point vibrometer. It contained an OFV505 vibrometer sensor head and an OFV-5000 modular vibrometer controller. Its sampling frequency was set to be 100 kHz. The grinding forces were measured by a Kistler four-component piezoelectric quartz crystal dynamometer (9272) and a charge amplifier (5070A). The ground

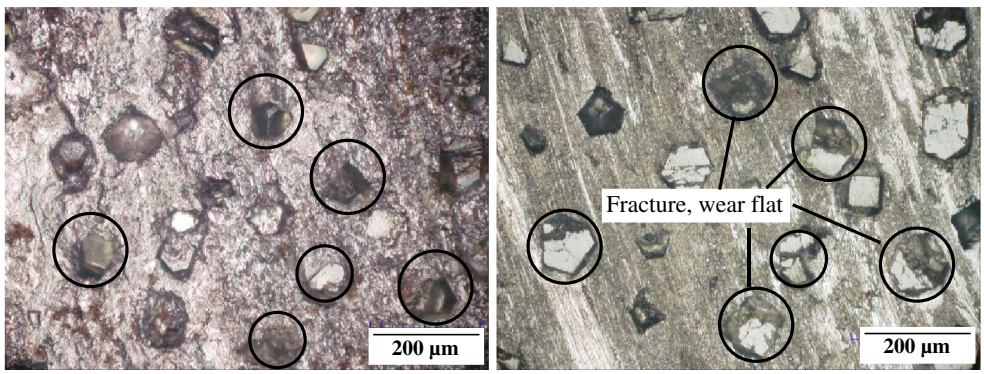


(a) Initial topography (b) Topography after 60 passes

**Fig. 6** Topography of the tool surface for UAG (×350). **a** Initial topography, **b** topography after 60 passes

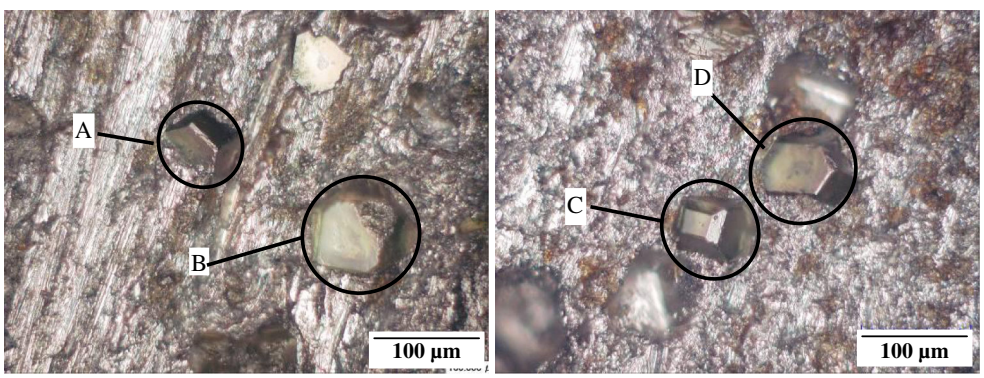


(a) CG (b) UAG

**Fig. 7** Initial state of the grains (×700). **a** CG, **b** UAG

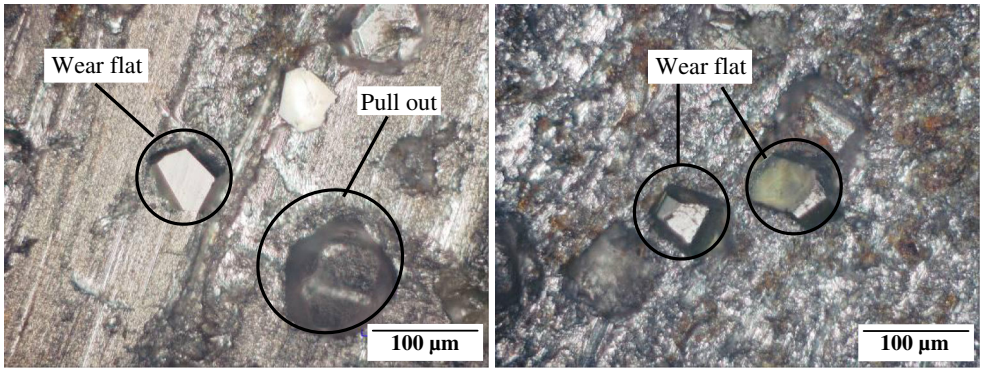


(a) CG (b) UAG

**Fig. 8** Topographies of the grains after grinding 20 passes (×700). **a** CG, **b** UAG

surface roughness was measured by a Mahr M1 instrument, and the measuring direction was vertical to the grinding direction. The micro-morphology of the grains and ground surface was observed by a Hirox KH-7700 optical microscopy after cleaning in acetone with a ultrasonic clean machine.

## 4 Experimental results and discussion

### 4.1 Topographic features of tool surface

Figures 5a and 6a show the grinding wheel topographies used in CG and UAG after the sharpening process and before any

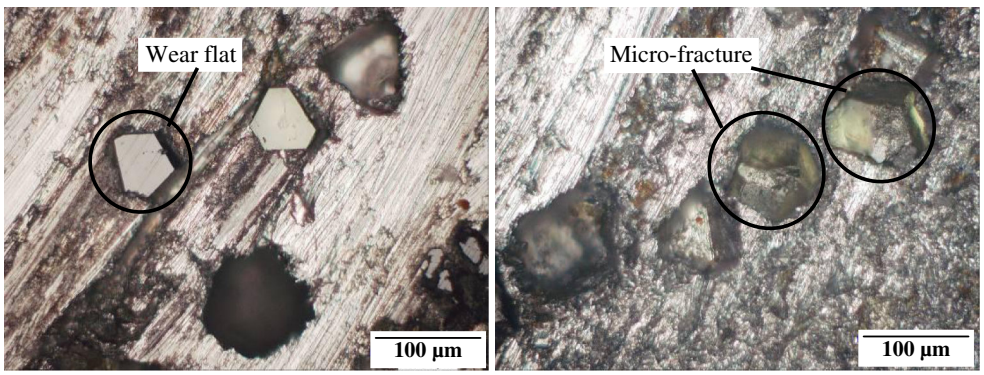


(a) CG (b) UAG

**Fig. 9** Topographies of the grains after grinding 40 passes (×700). **a** CG, **b** UAG

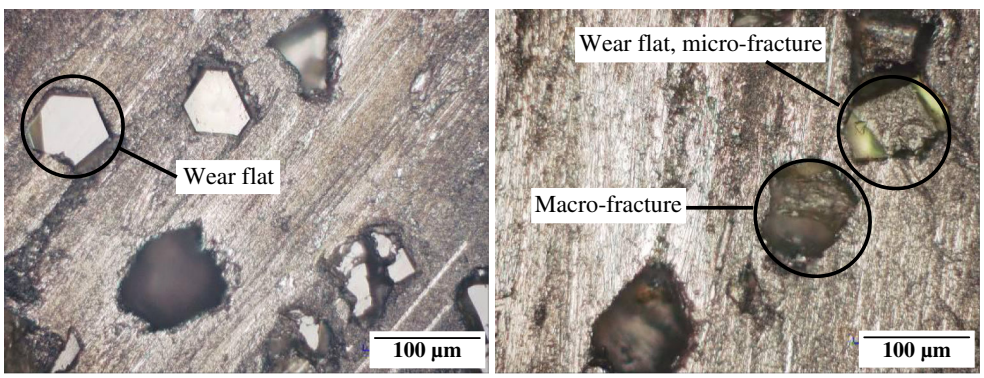


(a) CG (b) UAG

**Fig. 10** Topographies of the grains after grinding 60 passes (×700). **a** CG, **b** UAG

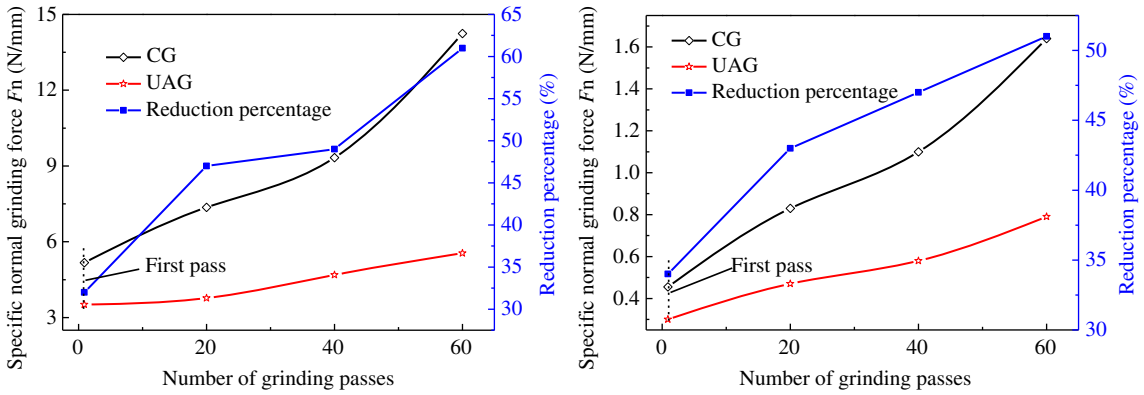


**Fig. 11** Grinding forces vs. number of grinding passes. **a** Specific normal grinding forces, **b** specific tangential grinding forces

grinding test is performed, respectively. It can be seen that their initial status is in accordance with each other. Figures 5b and 6b show the topographies of the two wheels after 60 grinding passes during CG and UAG, respectively. As seen from Fig. 5b, it is obvious that some grains are pulled out of the bonding agent. In addition, in nearly all the other grains, apparent wear flats were present which resulted from attritious wear. In comparison with CG, UAG (Fig. 6b) presents a different wheel surface topographic feature. Almost each grain possesses the micro-fracture, macro-fracture, and wear flats simultaneously. In addition, no pullout is observed during UAG under the experimental conditions. Due to the ubiquitous fracture feature of the grains, the grinding wheel during UAG can obtain more active cutting edge density compared with CG. The wear type of the bonding agent both in CG and UAG is attritious wear caused by the friction between the bonding agent and ground surface.

## 4.2 Wear processes of diamond grains

Figure 7 shows the initial topographies of the tracked grains, i.e., A and B in CG and C and D in UAG. Figures 8, 9, and 10 show their topographies after grinding 20, 40, and 60 passes, respectively. Compared with Fig. 7, it can be seen in Fig. 8 that a large-area wear flat appears in grain A, and grain B is pulled out during CG after 20 grinding passes, while only slight wear flats under the same conditions appear in grains C and D.

As can be seen in Fig. 9a, the wear flat of grain A enlarges during CG after 40 grinding passes. Meanwhile, the bonding agent begins to present obvious attritious wear resulting from severe attritious wear of the grains. However, a different phenomenon is observed during UAG, i.e., the micro-fracture appears on the surface of grains C and D. In this stage, it is obvious that better grinding ability could be kept in UAG than in CG. Then, after 60 grinding passes (see Fig. 10), the wear flat area of grain A in CG enlarges continuously and nearly has no protrusion; consequently, the wheel grinding ability becomes very poor. During UAG, a macro-fracture appears in grain C, and the wear flat of grain D enlarges which is accompanied with partial fracture on the edge area. In addition, it can be seen that the bonding agent of the grinding wheel also presents obvious attritious wear.

To sum up Figs. 8, 9, and 10, it can be seen that the wear processes of the grains during CG and UAG are different. During CG, grain pullout appears in the initial region of the grinding passes, and wear flat expands gradually during the whole process. Comparatively, the wear processes of the grains during UAG are slight attritious wear and micro-fracture, and there is a coexistence of macro-fracture and attritious wear at the end.

## 4.3 Grinding forces

The measured grinding forces versus the grinding passes during CG and UAG are shown in Fig. 11. The left *Y* axis denotes the measured values, and the right *Y* axis denotes the reduction percentage caused by UAG in comparison with CG. It is obvious that UAG can reduce both the specific normal grinding force and specific tangential force in comparison with CG under the same conditions. In addition, both the

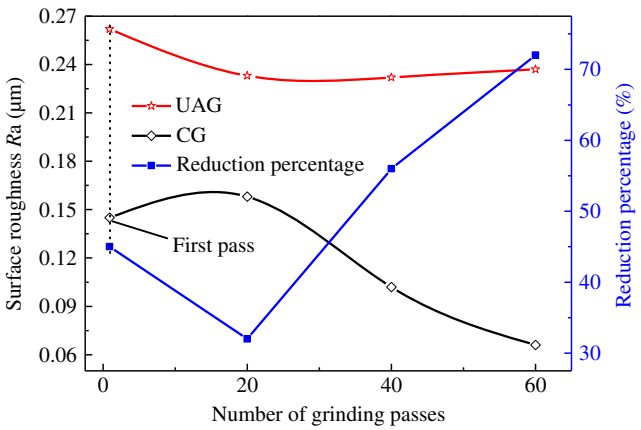


**Fig. 12** Ground surface roughness vs. number of grinding passes

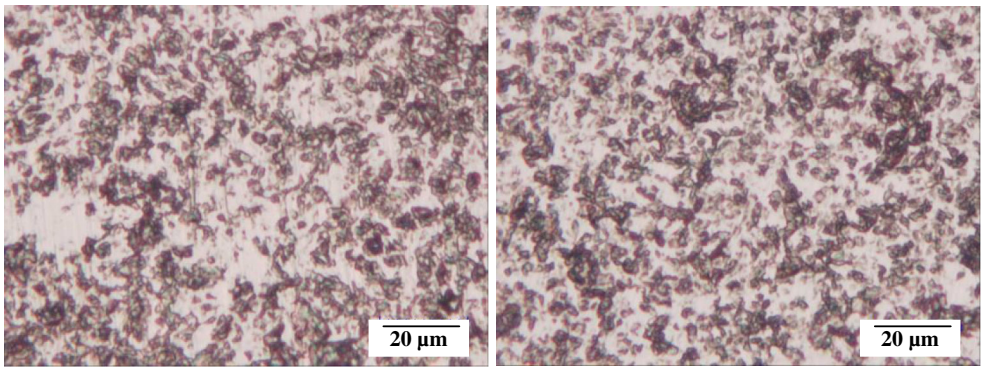


(a) CG: Ra 0.158 (b) UAG: Ra 0.233

**Fig. 13** Topographies of the ground surface after the first grinding pass (×2,800). **a** CG: Ra 0.158, **b** UAG: Ra 0.233

grinding forces during UAG and CG increase along with the increasing grinding passes.

As mentioned in Section 4.2, the tool wear processes during CG are pullout of grains, the appearance and expansion of the wear flats, and bonding attritious wear. Corresponding to this, the grinding forces increased rapidly along with the increase of the grinding passes. While in UAG, the tool wear process includes obvious more grain micro-fracture and macro-fracture besides wear flats and bonding attritious wear. Because of the grain fracture, the portion of grain splintering is assumed to be increased, i.e., more cutting edges become active. Thus, the grinding forces increase relatively slowly during UAG with the increase of the grinding passes compared with CG. For example, during the first pass, the specific normal grinding force and specific tangential grinding force obtained in UAG are decreased by 32 and 34 %, respectively, compared with that in CG, while the values change to 61 and 52 % during the 60th pass. Therefore, it can be inferred that it is much easier to keep the grinding wheel sharpness using UAG.

### 4.4 Ground surface roughness and topography

Figure 12 displays the variation of ground surface roughness with grinding passes during CG and UAG. The left *Y* axis denotes the measured values, and the right *Y* axis denotes the reduction percentage caused by CG in comparison with UAG. It can be seen that the ground surface quality in CG is better than that in UAG under the same conditions. With increasing grinding passes, the ground surface roughness obtained by CG first increases slightly in the beginning stages (0–20 grinding passes) and then decreases rapidly. However, the ground surface roughness obtained by UAG has no large fluctuation with increasing grinding passes and is always Ra 0.2–0.3 μm. Compared with UAG, the ground surface roughness obtained by CG is decreased by 32 % after grinding 20 passes, and the value can reach 72 % after grinding 60 passes.

Figures 13 and 14 illustrate the ground surface topographies obtained by CG and UAG after 20 and 60 grinding passes, respectively. Based on ground surface roughness, the topographies of the ground surface after 20 and 60 grinding passes have no significant difference in UAG. While in CG, the ground surface topography obtained after 60 grinding passes is much better than that obtained after 20 grinding passes.

### 4.5 Discussion

The changed motion characteristic of UAG causes the different grinding wheel wear characteristics, grinding forces, and ground

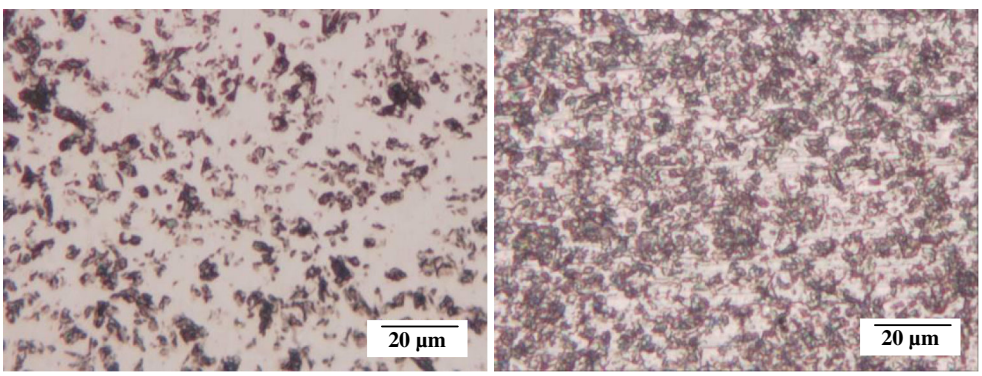


(a) CG: Ra 0.066 (b) UAG: Ra 0.237

**Fig. 14** Topographies of the ground surface after 60 grinding passes (×2,800). **a** CG: Ra 0.066, **b** UAG: Ra 0.237

surface quality in comparison with CG. Figure 15 shows the trajectory of a grain and its interaction with the workpiece during UAG. A motion cycle of the grain can be divided into two parts, i.e., $t_1$ and $t_2$. During $t_1$, the vibration speed $v_{UAG}$ vertical downward to the workpiece generates the hammering on the ground surface. In addition, the grinding speed $v_s$ parallel to the workpiece generates the grinding process. While during $t_2$, $v_{UAG}$ is vertical upward to the workpiece, namely, only the grinding works in this stage. Due to the hammering of grains, micro-fracture in the workpiece generates and prolongs easily. Accordingly, it is easier for a material to be removed in UAG than in CG. Thus, UAG can reduce the grinding forces effectively in the initial period under the same tool conditions. Consequently, it is easier for the grains to be pulled out (Fig. 8a) in CG because of larger grinding forces.

The effects of hammering and grinding on the grain wear processes are shown in Fig. 16. During the initial region (about 0–20 grinding passes) of UAG, the grinding process brings about attritious wear and generates the wear flats on the surface of the grains just as what occurred in CG. With the development (about 20–40 grinding passes) of UAG, micro-fracture generates gradually, resulting from the hammering. In the deteriorated region (about 40–60 grinding passes), the micro-fracture expands to the macro-fracture due to the accumulated hammering. Additionally, the initial wear flat also expands to a larger one because of the constant grinding as in CG. Consequently, the friction between the grains and workpiece is enhanced to some extent. This is the main reason for the increasing grinding forces during UAG.

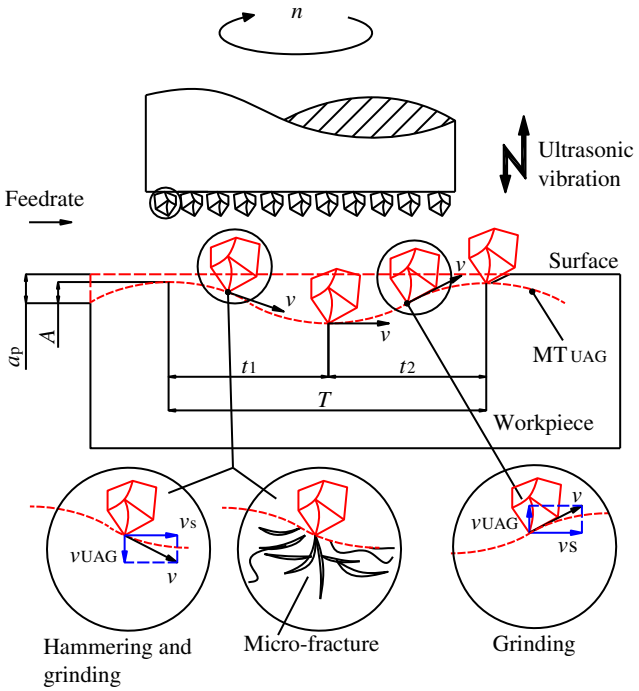


**Fig. 15** Hammering and grinding processes of the grains during UAG

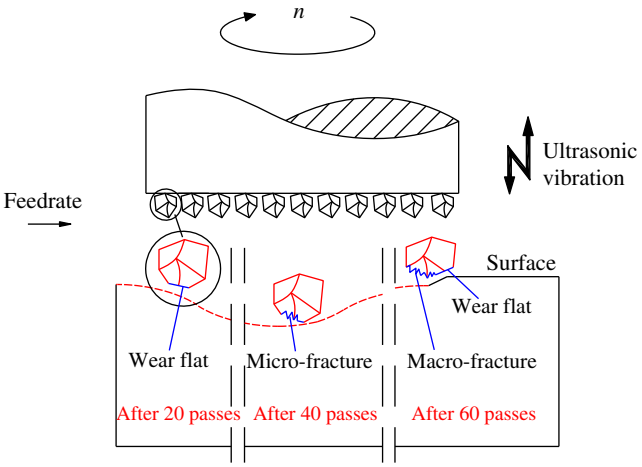


**Fig. 16** Illustration of the grain wear process during UAG

On the other hand, the contact status between the grains and workpiece also affects the wear patterns. In this study, the grinding depth $a_p$ (20 μm) is larger than the amplitude $A$ (4 μm). According to the kinematics analysis of UAG, although no complete contact disruptions between the grains and workpiece occurs, the contact area $S_{UAG}$ between them changes all the time as illustrated in Fig. 17. While in CG, the contact area $S_{CG}$ maintains constant. Consequently, the grinding wheel during UAG undertakes impulsive load and alternating load that result from regular changing of $S_{UAG}$ and then the micro-fracture and macro-fracture of grains are promoted to generate. Thus, more cutting edges become active, and the grinding wheel keeps sharpening due to lower frictional effects. Accordingly, the grinding forces are lower and have no remarkable fluctuation with increasing grinding passes. However, the grinding wheel during CG undertakes relatively stable grinding forces, and attritious wear is dominant that causes sustainable enlarging of the wear flat. As a result, the grinding wheel becomes blunt, and the grinding forces increase rapidly with increasing grinding passes.

Motion trajectory and wear patterns of grains also affect the ground surface quality significantly. Due to the hammering generated by ultrasonic vibrations, higher grain penetration happens and more micro-pits originate during UAG than during CG. Thus, UAG obtains slightly rougher finished surface in the initial period when the two wheels have nearly the same status. With increasing grinding passes, the grinding ability of the wheel in UAG varies slightly and produces stable ground surface roughness. However, due to more serious attritious wear with increasing grinding passes in CG, it is more difficult for the grains to penetrate into the workpiece and more scratching occurs. Consequently, CG obtains smoother ground surface than UAG, especially in the later stage of the wear process.

Generally speaking, compared with CG, UAG can reduce the grinding force effectively with slightly rougher ground surface when the grinding wheel is in normal status. Besides, UAG can maintain the grinding wheel sharpening

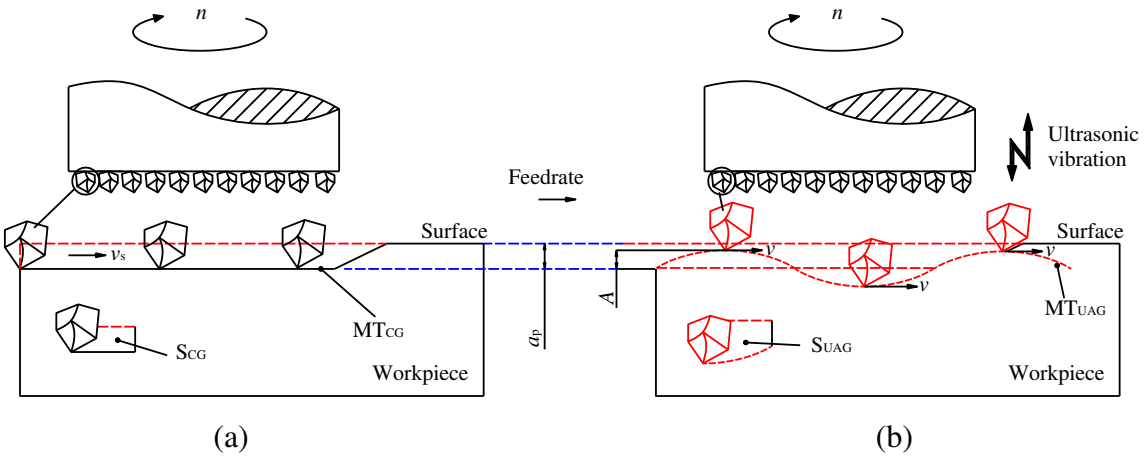


**Fig. 17** Comparison of contact area between **a** CG and **b** UAG

for longer time than CG; accordingly, the dressing times can be reduced. Thus, for ceramic materials like SiC, UAG can be applied as a highly effective production technology.

## 5 Conclusions

Wear behavior of the sintered cup diamond wheel and its effects on the grinding force and ground surface quality during UAG have been studied through comparative experiments with CG. The following conclusions can be drawn based on the experiment results:

1. During UAG, the micro-fracture and macro-fracture of the diamond grains were the main wear patterns accompanied with partial wear flat, while attritious wear was the dominant wear pattern during CG.
2. Due to grain fracture, more cutting edges became active, and the grinding wheel kept sharpening during UAG. Accordingly, UAG can reduce the grinding forces effectively in comparison with CG, especially with the development of the grinding process.
3. Compared with CG, UAG obtained slightly rougher ground surface results from higher grain penetration and more micro-pits caused by hammering.

**Acknowledgments** The authors would like to gratefully acknowledge the support of the National Natural Science Foundation of China (grant no. 51275231) and Fundamental Research Funds for the Central Universities (grant no. CXLX11_0173).

## References

1. Ji RJ, Liu YH, Zhang YZ, Cai BP, Ma JM, Li XP (2012) Influence of dielectric and machining parameters on the process performance for electric discharge milling of SiC ceramic. Int Adv Manuf Technol 59: 127–136
2. Wang XZ, Wang J, Wang H (2012) Preparation of high-temperature organic adhesives and their performance for joining SiC ceramic. Ceram Int 39:1365–1370
3. Ni JM, Li BZ (2012) Phase transformation in high-speed cylindrical grinding of SiC and its effects on residual stresses. Mater Lett 89: 150–152
4. Zhong Z, Nakagawa T (1996) Grinding of aspherical SiC mirrors. J Mater Process Technol 56:37–44
5. Agarwal S, Rao P (2008) Experimental investigation of surface/subsurface damage formation and material removal mechanisms in SiC grinding. Int J Mach Tools Manuf 48:698–710
6. Malkin S, Hwang TW (1996) Grinding mechanisms for ceramics. CIRP Ann 45(2):569–580
7. Liang ZQ, Wang XB, Wu YB, Xie LJ, Liu ZB, Zhao WX (2012) An investigation on wear of resin-bonded diamond wheel in elliptical ultrasonic assisted grinding (EUAG) of monocrystal sapphire. J Mater Process Technol 212:868–876
8. Hosokawa A, Ueda T, Yunoki T (2006) Laser dressing of metal bonded diamond wheel. Ann CIRP Manuf Technol 55(1):329–332
9. Liu DF, Cong WL, Pei ZJ (2012) A cutting force model for rotary ultrasonic machining of brittle materials. Int J Mach Tools Manuf 52: 77–84
10. Bahman A, Taghi T (2011) Development of a novel ultrasonic unit for grinding of ceramic matrix composites. Int Adv Manuf Technol 57:945–955
11. Christian B, Ralf S, Andreas W, Christian W, Sophia H (2010) New systematic and time-saving procedure to design cup grinding wheels for the application of ultrasonic-assisted grinding. Int Adv Manuf Technol 47:153–159
12. Ishikawa K, Suwabe H, Nishide T, Uneda M (1998) A study on combined vibration drilling by ultrasonic and low-frequency vibrations for hard and brittle materials. Precis Eng 22:196–205
13. Peng Y, Wu YB, Liang ZQ, Guo YB, Lin X (2011) An experimental study of ultrasonic vibration-assisted grinding of polysilicon using two-dimensional vertical workpiece vibration. Int Adv Manuf Technol 54:941–947
14. Wang X, Zhou M, Gan JGK, Ngoi B (2002) Theoretical and experimental studies of ultraprecision machining of brittle materials with ultrasonic vibration. Int Adv Manuf Technol 20:99–102
15. Liang ZQ, Wu YB, Wang XB, Zhao WX (2010) A new two-dimensional ultrasonic assisted grinding (2D-UAG) method and its fundamental performance in monocrystal silicon machining. Int J Mach Tools Manuf 50:728–736
16. Uhlmann E (1998) Surface formation in creep feed grinding of advanced ceramics with and without ultrasonic assistance. Ann CIRP Manuf Technol 47(1):249–252

17. Yan YY, Zhao B, Liu JL (2009) Ultraprecision surface finishing of nano-$ZrO_2$ ceramics using two-dimensional ultrasonic assisted grinding. Int Adv Manuf Technol 43:462–467
18. Malkin S (1989) Grinding technology: theory and applications of machining with abrasives. Ellis Horwood, Chichester, pp 197–221
19. Zeng WM, Li ZC, Pei ZJ, Treadwell C (2005) Experimental observation of tool wear in rotary ultrasonic machining of advanced ceramics. Int J Mach Tools Manuf 45:1468–1473
20. Mult HC, Spur G, Holl SE (1996) Ultrasonic assisted grinding of ceramics. J Mater Process Technol 62:287–293